



46th SME North American Manufacturing Research Conference, NAMRC 46, Texas, USA

# A Model for Predicting the Geometry of Crater on Grinding Wheel Surface Ablated with a Single Pulsed Laser

Uma Shankar<sup>a</sup>, N. Ramesh Babu<sup>b,\*</sup>

<sup>a</sup>Research Scholar, Manufacturing Engineering Section, Mechanical Engineering Department, IIT Madras

<sup>b</sup>Professor, Manufacturing Engineering Section, Mechanical Engineering Department, IIT Madras

\* Corresponding author. Tel.: +91-44-2257-4675.  
E-mail address: [nrbabu@iitm.ac.in](mailto:nrbabu@iitm.ac.in)

## Abstract

In this paper, a three dimensional transient heat transfer model for predicting the 3D geometry of crater and its cross sectional profile on grinding wheel surface ablated by a single pulsed Nd: YAG laser is covered. The model considers the heterogeneity of wheel structure, the variation of energy in a pulsed laser input to the wheel, heat transfer by conduction, convection, radiation and the thermo-physical and optical properties of bond and grit while predicting the temperature distribution in the irradiated region using COMSOL Multiphysics<sup>®</sup> 5.2 package. From this temperature distribution, the shape of crater was predicted. Crater depth predicted was validated with the published results confirming the suitability of this model for predicting the shape of crater in single pulsed laser ablation of wheel surface. Post modeling analysis gives insights of the process mechanism of laser dressing and the parameters affecting the crater geometry. Future scope and implementation of this model is discussed in detail.

© 2018 The Authors. Published by Elsevier B.V.

Peer-review under responsibility of the scientific committee of the 46th SME North American Manufacturing Research Conference.

*Keywords:* laser dressing of grinding wheels; wheel structure model; single-pulse laser ablation; crater geometry.

## 1. Introduction

In grinding process, the wheel continuously interacts with the work surface in order to generate the desired finish on its surface. During grinding, a grinding wheel undergoes wear such as bond fracture,

grain fracture, grain pull-out, etc. which leads to the degradation of wheel topography and form. This, in turn, produces inconsistent results in grinding. For realizing consistent results in grinding, the wheel is periodically subjected to dressing to rejuvenate the wheel sharpness and trueness. Normally, a single point diamond dresser or diamond disc is used for dressing

of grinding wheels. Due to its contact nature, the diamond dresser wears out continuously and thus influences the topography on dressed wheel [1]. Besides this, it causes excessive wheel loss due to grit pull out [2]. The wear on dresser is more while dressing of superabrasive wheels, owing to their hardness, as compared to conventional wheels. In order to realize consistency in dressing of wheels, several unconventional methods such as electrolytic in-process dressing, electro discharge machining, electro chemical machining, abrasive waterjet based dressing, etc. were explored. Most of these approaches of dressing are limited to a particular type of wheel system besides requiring a special set up. Laser dressing of grinding wheels, being a non-contact method, facilitates the ease of removal of material irrespective of the type of wheel and possesses certain merits such as profile dressing and structuring which is difficult with conventional and other unconventional methods of dressing [3].

Laser dressing of grinding wheels was first investigated in the late 1980 [3, 4]. The idea that laser can be used for micron level material removal inspired the researchers to investigate the feasibility of dressing wheels using laser beam. Over a period of the last three decades, both continuous wave as well as pulsed lasers of pulse widths ranging from picosecond to microsecond were investigated for dressing of various grinding wheels. The results of laser dressing experimentation from the past research is summarized in Section 2 of this paper. The process of laser dressing is fundamentally different from the traditional approach of dressing of grinding wheels. It is based on the principle of removing material from wheel surface using a laser beam with a suitable power density.

The process mechanism is based on laser-wheel material interaction leading to heating, melting, vaporization, plasma formation, ablation of grits and bond, etc. Besides the beam power density, the pulse width also determines the regime of material removal of bond and grit. In case of laser beam of picosecond pulse width, the material removal takes place by photo ablation mechanism whereas lasers of nanosecond and millisecond pulse widths involve vaporization and melt expulsion mechanism. The extent of material removal from grinding wheel depends on the laser power density as well as the focal offset distance [5, 6]. The principle of laser dressing of grinding wheels is shown in the schematic sketch in Fig. 1. When a pulsed laser beam interacts with the wheel surface, craters are created due to material removal by each pulse. Due to

the relative motion of the focused laser spot over the revolving wheel surface, the craters formed by subsequent pulses overlap both in axial and circumferential direction, leading to the removal of wheel material from its surface. The crater geometry not only defines the amount of wheel material removal but also influences the topography generated on the wheel. The laser parameters like average power, pulse repetition rate, pulse width, etc. affects the crater geometry and thus the topography on laser dressed wheel.

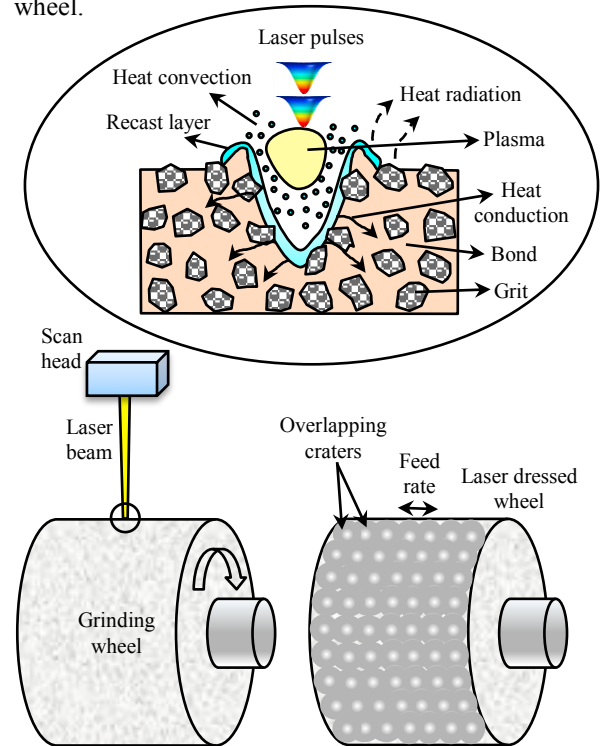


Fig. 1. Schematic of the principle mechanism in laser dressing

Modeling of laser ablation of wheel surface requires geometric representation of wheel structure and heat transfer modeling to generate temperature distribution due to laser-wheel interaction. Previous models were limited in modeling wheel structure as the grits were assumed to have symmetrical shape and size and porosity was neglected [27, 28, 29]. The thermal analysis was based on finite difference approach but it could not consider all the physical phenomena like heat conduction, convection, radiation, phase change, plasma formation, etc.

In order to accurately predict the geometry of crater on grinding wheel surface by laser pulse ablation, the physical structure of wheel consisting of the geometrical features of grits, bond and porosity in a

localized region is important and was covered. This paper aims at the development of thermal model for predicting the geometry of crater formed by a single-pulse laser ablation on resin bonded superabrasive wheels. Based on this model, the influence of laser parameters and the wheel properties on the crater geometry and the topography of the laser dressed grinding wheels was studied. The modeling work is covered in two parts. First, the geometric structure of the grinding wheel based on its specifications like grit size and volume fractions of grit and bond is modeled using the framework presented in [33]. The second part covers the development of a 3 D transient heat model which incorporated a single pulsed laser ablation mechanism in order to obtain crater geometry. The modeling results are validated with the published data [5].

## 2. Literature Review

### 2.1. Review of experimental work on laser dressing of grinding wheels

In 1989, the investigation on laser dressing of vitrified aluminum oxide grinding wheel was carried out using Nd:YAG laser of wavelength  $1.06\ \mu\text{m}$  and pulse width  $460\ \mu\text{s}$  and the microstructural features of laser dressed wheel surface such as craters and smooth recast layer with multiple cracks were reported [3, 4]. Wheel topography was influenced by feed rate at a particular intensity. Although fine topography was obtained at an intensity of  $6 \times 10^{10}\ \text{W}/\text{m}^2$  and a feed rate of  $0.35\ \text{mm}/\text{rev}$ , the grinding forces and surface finish showed opposite trend [4]. Laser fluence was found to influence surface morphology of laser dressed alumina wheels [7, 8]. The presence of densified surface and subsurface with preferentially oriented multifaceted grain having well-defined cutting edges and vertices was reported in laser dressed alumina wheels [8, 9, 10]. Resin bonded CBN wheel was laser dressed and the groove geometry was optimized by selecting appropriate laser dressing parameters like laser power density, spot diameter, scan speed and overlap coefficient [11, 12]. The temperature signals showed favorable result in grinding using laser dressed wheel as compared to mechanically dressed wheel. Acousto-Optic Q-switched laser with high peak power and short pulse duration was applied for selective removal of resin bond to generate a suitable topography on the wheel [5, 6]. The grinding behavior

of a resin bonded CBN grinding wheel led to 10-15% decrease in grinding forces in grinding hardened block steel as compared to corundum block-dressed wheels. However, there was no attempt to investigate the surface finish of workpiece ground using laser dressed resin bonded CBN wheels. In laser dressing of segmented metal bonded diamond wheels, the process became efficient at higher speed and by using air jet that could blow away the molten bond material [13]. Micro-wheels with ultra-fine diamond grit dressed using Nd:YAG laser of wavelength  $355\ \text{nm}$  produced better surface finish in grinding of micro-aspherical optics and cutting edge density increased up to 2.5 times higher than conventional dressing method [14]. A resin bonded diamond wheel was dressed up to  $2\ \mu\text{m}$  depth using a newly developed UV laser with multi-mode fiber optics [15]. However, the laser dresser was not suitable for industrial application because of its long dressing time of about 2 hours. In laser dressing of metal bonded diamond wheel, grit protrusion height of  $80\text{--}90\ \mu\text{m}$  was obtained as compared to  $50\text{--}60\ \mu\text{m}$  in mechanical dressing [16]. Besides this it also exhibited longer life of 50 hours while grinding Nickel based superalloy (IN 718) as compared to 25 hours with mechanically dressed wheel. No thermal damage was observed on the diamond grit and the recast layer formed over bond was removed during grinding operation. Metal-vitrified hybrid bonded CBN wheels were dressed using short pulse fiber laser [17, 18]. Better grit protrusion height could be achieved in a single pass for pulse energy less than  $1\ \text{mJ}$  [17]. In grinding of 100Cr6 hardened bearing steel, the forces using the laser dressed wheel were lesser than the conventionally SiC dressed wheel. However, the surface finish and the wheel wear rate during grinding were undesirable for laser dressed wheel [17]. Laser dressing of bronze bonded diamond grinding wheel using pulsed Yb:YAG laser was optimized with respect to laser power density, pulse overlap, line overlap and the number of scanning cycles to achieve lesser grinding forces [19]. Laser beam of intensity  $1.68 \times 10^8\ \text{W}/\text{cm}^2$  could perform only dressing,  $2.52 \times 10^8\ \text{W}/\text{cm}^2$  combined both truing and dressing and  $3.36 \times 10^8\ \text{W}/\text{cm}^2$  could do ultra-depth dressing which was found undesirable [20, 21]. The phenomena of the phase explosion of bronze bond yielded undesirable grinding results and was minimized by using power density in the range of  $18.37 \times 10^7\text{--}20.99 \times 10^7\ \text{W}/\text{cm}^2$  [22]. Nano second fiber laser of average power  $20\ \text{W}$  was used for normal and quasi-tangential profiling of

bronze bonded diamond and porous aluminium oxide grinding wheels [34]. The material removal rate and profile accuracy was found to depend strongly on the angle of laser beam incidence. Besides, this, the profile accuracy can be improved by using shielding gas.

## 2.2. Review of modeling work on laser dressing of grinding wheels

Various approaches were used to model laser dressing of grinding wheels. A major part of the research on laser conditioning of grinding wheels is based on empirical investigation of the process feasibility. These empirical studies were aimed to understand the characteristics of laser dressed wheel such as microstructural features, surface topography and the performance of laser dressed wheels in comparison to the conventionally dressed wheels. However considering the complexities of the process mechanism and the vast number of parameters affecting laser dressing process, there were no attempts to model the process output in terms of process parameters though efforts were made to study the process behavior using statistical approaches. Physical modeling of the process was attempted by considering the physical phenomena such as heat transfer, phase change, hydrodynamics, etc. The approaches used were either analytical, numerical such as finite difference method or finite element method or integrated computational and experimental method. The analytical model employed energy principles to analyze the heat inputs by the laser to the grinding wheel surface. An energy model was developed for laser dressing of a small vitrified bonded CBN grinding wheel to predict the effect of incidence angle, focal offset, laser power density and scan speed on the absorbed energy and volume of material removed [23, 24]. In another attempt, the efficiency of laser dressing was analyzed through modeling based on energy principle that used both geometrical as well as numerical modeling [25]. Analysis of thermal based phenomena during laser interaction with wheel material yields the partial differential equation which can be solved for the temperature distribution in the wheel material. This type of problem is attempted by numerical modeling approaches.

Thermal analysis of laser conditioning of grinding wheels considering the heat transfer phenomena such as heat conduction, convection and radiation is analyzed as a heat transfer problem during each pulse

duration ( $t_p$ ) and three dimensional heat transfer equations are given [26].

Heat conduction equation:

$$\frac{\partial T(x, y, z)}{\partial t} = \alpha(T) \nabla^2 T(x, y, z, t) \quad (1)$$

where

$$\nabla^2 = \frac{\partial^2}{\partial x^2} + \frac{\partial^2}{\partial y^2} + \frac{\partial^2}{\partial z^2}$$

and  $\alpha(T)$  is the temperature dependent thermal diffusivity of wheel material.

Heat convection and radiation equations:

$$-k(T) \left[ \frac{\partial T(x, y, 0)}{\partial x} + \frac{\partial T(x, y, 0)}{\partial y} + \frac{\partial T(x, y, 0)}{\partial z} \right] \quad (2)$$

$$= -\delta P + h[T - T_a] + \varepsilon \sigma [T^4 - T_a^4]$$

where  $h$  – the convection heat transfer coefficient,  $T_a$  – ambient temperature,  $\delta = 1$  for single pulse duration,  $\varepsilon$  – surface emissivity,  $\sigma$  – Stefan–Boltzmann constant ( $5.67 \times 10^{-8} \text{ W/m}^2 \text{ K}^4$ ) and  $P$  – the laser power density given by,

$$P = AP_p e^{-\left[ \frac{(x-x_0)^2 + (y-y_0)^2}{2\phi^2} \right]} \quad (3)$$

where  $\phi$  is the standard deviation of Gaussian beam profile and  $x_0$  and  $y_0$  are the coordinate points of the centre of laser spot,  $A$  is the absorptivity of laser by the wheel material and  $P_p$  is the peak power density given by,

$$P_p = \frac{4P_a}{\pi D^2 f t_p} \quad (4)$$

where  $P_a$  – average laser power,  $D$  – laser spot diameter,  $f$  – pulse frequency and  $t_p$  – pulse width of the laser. Also the dynamics of phase change, fluid mechanics, plasma formation and shock wave propagation need to be modeled along with heat transfer.

The previous attempts to develop thermal models of laser conditioning of grinding wheels suffer from many limitations such as simplification of the problem by neglecting phenomena such as heat convection and radiation, hydrodynamics of fluid flow, plasma formation, recoil pressure and shock wave propagation [27, 28, 29]. One of the major drawback of these models is that the structure of grinding wheels subjected to thermal analysis were limited by approximating it as a simple cubic structure with spherical shaped grits without any porosity [27, 28].

An attempt was made to capture the complexity of the physical phenomena such as energy absorption, heat transfer and latent heat mechanism, the three phase interactions, surface tension, the vaporization-induced recoil force, the thermal buoyancy force and Darcy friction in single pulsed laser ablation of bronze bonded diamond wheel [30]. An integrated approach was used to develop a computational model which could predict the surface roughness over laser dressed alumina ceramics for given laser machining conditions. It was developed based on the physical phenomena like heat transfer, recoil pressure, surface tension, etc. using the package COMSOL Multiphysics® [26]. However the model was limited to a single material domain and did not consider the heterogeneity of grinding wheel structure such as grits, bond and porosity.

Considering the complex nature of laser dressing of grinding wheels, the experimental investigations may be limited to capturing the effects of various

parameters on the process output. The approach of physical modeling of laser dressing process and predicting the process output like surface topography of wheel gives insights of the process mechanism and can be helpful to determine the ranges of laser dressing process parameters for a particular grinding application like ultrafine-finish, finish or rough grinding. Most of the research on laser conditioning of grinding wheels involved post process analysis like microstructural analysis of laser dressed wheels, study on surface topography and performance analysis during grinding. However, much of the cost, resource and time can be saved by the means of modeling and simulation of the process using an appropriate strategy. In this work, a suitable framework is developed to model the crater geometry in laser dressing of grinding wheels, which can be further extended to model the topography of wheel generated by laser dressing with certain input conditions.

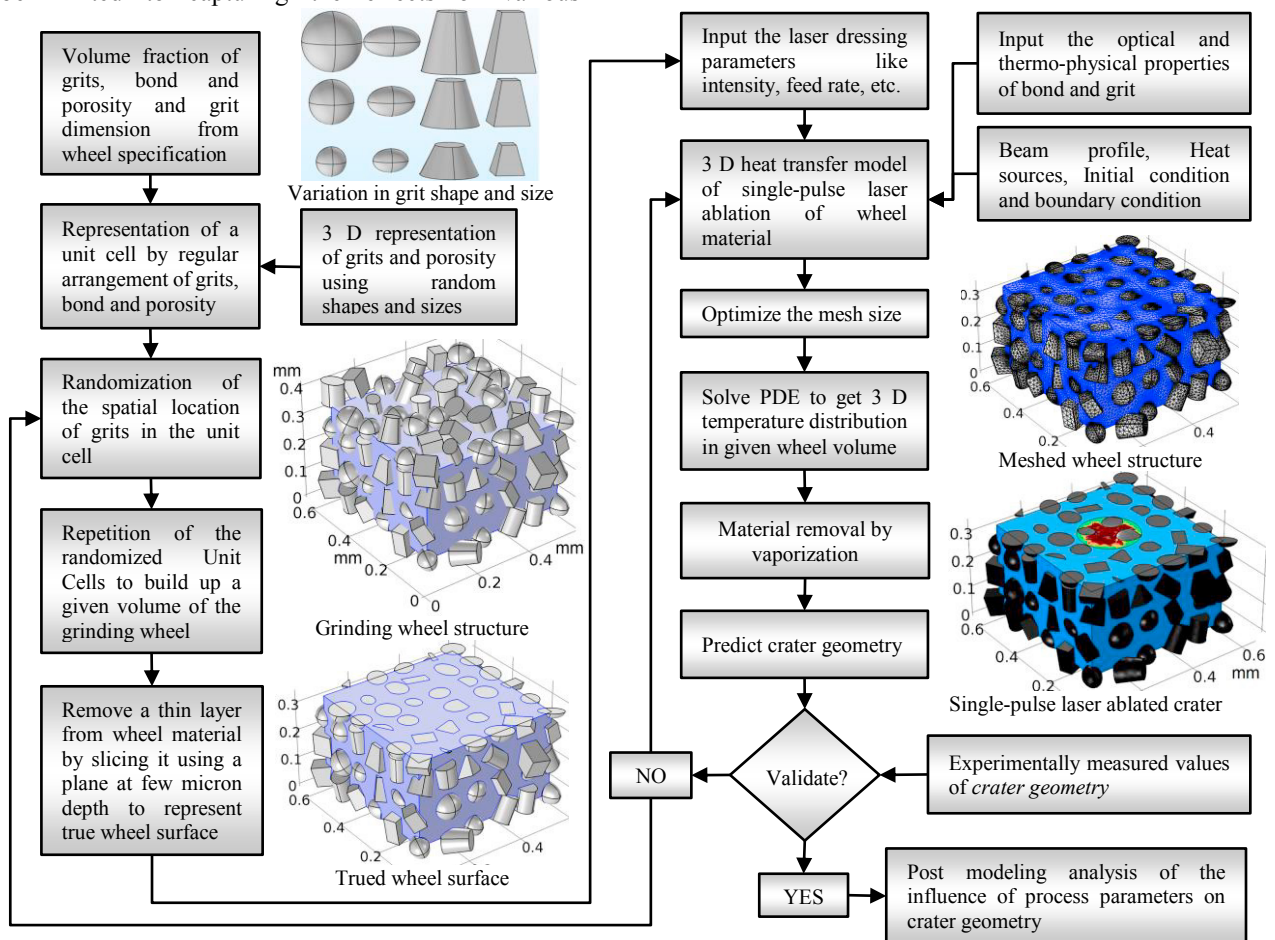


Fig. 2. Framework for modeling the crater geometry in single-pulse laser ablation

### 3. Framework to model the crater geometry using single-pulse laser ablation of grinding wheels

The framework shown in Fig. 2 consists of two stages of modeling. In the first stage, a model of wheel structure was developed representing the grits of irregular shapes and size distributed in the bond material. Also this model is generalized to accommodate various bonded abrasives including porous wheels. This model is implemented using COMSOL 5.2 with MATLAB platform.

Using this geometric model of the wheel, post processing is done in the geometry node of COMSOL Multiphysics® 5.2 to generate a trued wheel surface. Later this is used for thermal modeling of irradiated zone where the trued wheel surface is exposed to laser beam with given conditions of laser dressing like average power, pulse width, pulse repetition rate, focal distance, etc. Based on the physical phenomena, a transient heat transfer model is developed considering individual material properties of grits and bond. By applying the boundary conditions and refining the mesh, the temperature distribution in the wheel was obtained. While post processing, the mesh elements with temperature higher than the ablation temperature of grits and bond were removed from the respective domains to obtain the geometry of crater. The procedure of modeling is outlined in the next section.

#### 3.1. Modeling of grinding wheel structure

It is important to model the wheel structure precisely as the distribution of grits in the bond affects the localized material removal by laser dressing owing to different optical and thermo-physical properties of constituents, which in turn influence the formation of crater during laser-wheel material interaction.

From the specifications of a grinding wheel such as grit number ( $M$ ), structure number ( $S$ ) and grade number ( $n$ ), the average grit dimension ( $D_g$ ) and the volume fractions of grit ( $V_g$ ), bond ( $V_b$ ) and porosity ( $V_p$ ) can be derived using empirical equations as given below based on literature [31]:

$$D_g = \frac{15.2}{M} \tag{5}$$

$$V_g = \frac{2(32-S)}{100} \tag{6}$$

$$V_p = \frac{2(99.5-2n)-100V_g}{300} \tag{7}$$

From the geometry of the unit cell as shown in Fig. 3, the size of unit cell ( $a$ ) and spherical pore ( $D_p$ ) is given by,

$$a = D_g \left( \frac{\pi}{6V_g} \right)^{\frac{1}{3}} \tag{8}$$

$$D_p = a \left( \frac{6V_p}{\pi} \right)^{\frac{1}{3}} \tag{9}$$

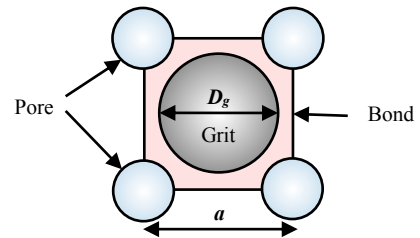
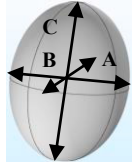
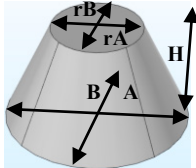
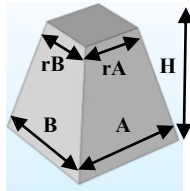


Fig. 3. Simple cubic unit cell containing grit, bond and porosity

Table 1. Selection of various grit shapes

S. No.	Grit Shape	Parameters
1	Ellipsoid 	$A = kD_g, B = \frac{D_g}{k}$ $C = D_g$ $k \geq \frac{D_g}{a}$
2	Frustum 	$A = k_1D_g, B = k_2D_g$ $H = D_g$ $r = \frac{\sqrt{\frac{8}{k_1k_2} - 3} - 1}{2}$ $k_1k_2 \geq 0.67$ for $r \leq 1$
3.	Truncated pyramid 	$A = k_1D_g, B = k_2D_g$ $H = D_g$ $r = \frac{\sqrt{\frac{2\pi}{k_1k_2} - 3} - 1}{2}$ $k_1k_2 \geq \frac{\pi}{6}$ for $r \leq 1$

In modeling of wheel structure, first the geometrical shape of grit were selected. The grit shapes are assumed to be polyhedral such as frustum and truncated pyramid besides spherical and ellipsoidal shapes. In the literature, grits of spherical

shapes were assumed to be arranged in a simple cubic structure. Assuming the base shape of grit as sphere with diameter  $D_g$  (the mean grit dimension), different grit shape factors ( $k$ ) were derived considering the grits to have same volume as the base sphere. Based on the geometrical analysis the shape parameters of different shaped grits are determined and are shown in Table 1.

Generally the size of grits exhibit normal distribution between maximum and minimum dimension. For a given grit number ( $M$ ), the extreme values can be obtained from [32].

$$D_{\min} \leq D \leq D_{\max}$$

$$D = kD_g \quad (10)$$

where  $k$  is the size factor given by,

$$k = \frac{D_{\min}}{D_g} + R_n \left( \frac{D_{\max} - D_{\min}}{D_g} \right) \quad \forall R_n \in N(0,1)$$

In order to maintain the same volume fraction of grit in a given volume of wheel material, the grit sizes are varied about the mean grit dimension in a pairwise manner in consecutive unit cells as given below and shown in Fig. 4.

$$D_1 = k_1 D_g \text{ and } D_1' = (2 - k_1^3)^{\frac{1}{3}} D_g$$

$$D_2 = k_1 D_g \text{ and } D_2' = (2 - k_1^3)^{\frac{1}{3}} D_g \text{ and so on,}$$

where  $k_1, k_2, \dots$  are the random size factors.

The location of grits were randomized from the uniform structure by giving random displacements to grit centers within each unit cell. To randomize a grit in the  $n^{\text{th}}$  unit cell, the final coordinates are given by,

$$X = n \frac{a}{2} + R_n \Delta x \quad (11)$$

$$Y = n \frac{a}{2} + R_n \Delta y \quad (12)$$

$$Z = n \frac{a}{2} + R_n \Delta z \quad (13)$$

where  $R_n$  is the random fraction and  $\Delta x, \Delta y$  and  $\Delta z$  are the separation between grit and pore in the axes directions within a unit cell.

Using the above methodology, a given volume of the selected resin bonded superabrasive grinding wheels were generated using the MATLAB interface of COMSOL Multiphysics<sup>®</sup>. The geometric model was then imported into the COMSOL end where a thin layer of 50  $\mu\text{m}$  was removed to represent a trued wheel surface before subjecting it to pulsed laser radiation.

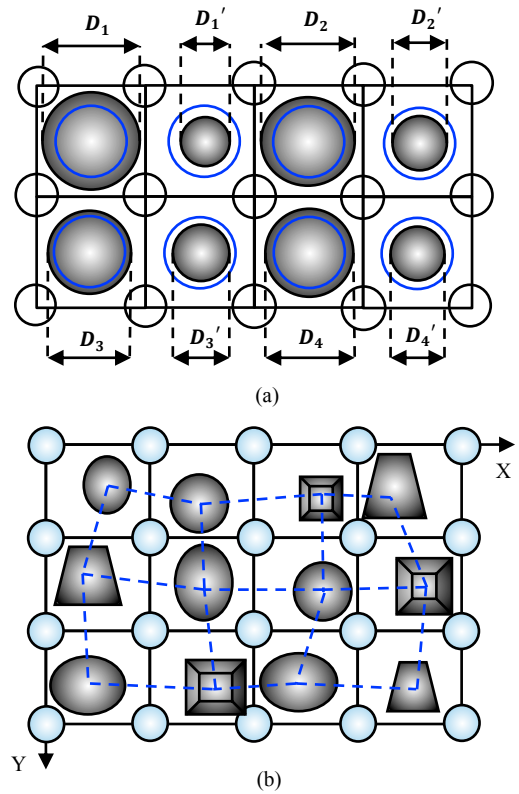


Fig. 4. (a) Variation of grit size of base shape sphere (b) Variation of grit location

### 3.2.3 $D$ transient thermal model for predicting temperature distribution in single-pulse laser ablation of grinding wheel

The transient thermal model was implemented at COMSOL Multiphysics<sup>®</sup> 5.2. Various assumptions made in developing the model include:

- Beam profile of laser is considered to be Gaussian.
- The variation of thermal conductivity and specific heat at constant pressure of resin bond with temperature is neglected.
- The time period of study is one-pulse duration.
- The intensity applied is only for the condition of laser dressing, i.e. applied intensity is above the threshold intensity of resin bond and below that of CBN and diamond grits.
- Surface tension effects due to the molten phase of grit and bond are neglected.
- Cooling effect due to coaxial gas is neglected.
- Plasma formation and shielding effect are neglected.

Table 2. Input parameters to the heat transfer model

S. No	Parameter	Values
1	Average power ( $P_a$ )	3 W
2	Beam diameter ( $D$ )	0.20 mm
3	Pulse width ( $t_p$ )	150 ns
4	Pulse repetition rate ( $f$ )	1 kHz
5	Peak power ( $P_p$ )	$4P_a/(\pi.f.t_p.D^2)$
6	Standard deviation of Gaussian beam profile ( $\phi$ )	$D/6$

Table 3. Properties of grits and bond

S. No	Property	Resin (phenolic)	CBN	Diamond
1	Density ( $\text{kg/m}^3$ )	1340 [35]	3487 [36]	3515 [36]
2	Specific heat ( $\text{J}/(\text{kg.K})$ )	1400 [37]	505.687 [47]	515.897 [36]
3	Thermal conductivity ( $\text{W}/(\text{m.K})$ )	0.25 [37]	1300 [38]	2000 [39]
4	Absorptance at 1064 nm	0.8 [5]	0.3 [40]	0.16 [40]
5	Surface emissivity	0.8 [41]	0.8 [42]	0.81 [43]
6	Thermal behaviour	In inert atmosphere, it decomposes above 573 K, changes into glassy state above 773 K and becomes gases from 673 – 973 K [45].	Melting at 3246 K [44]	Melting at 4100 K [44]
7	Heat convection coefficient	100 [46]	100 [46]	100 [46]

Assumptions (b), (d), (e) and (f) are made due to lack of literature data.

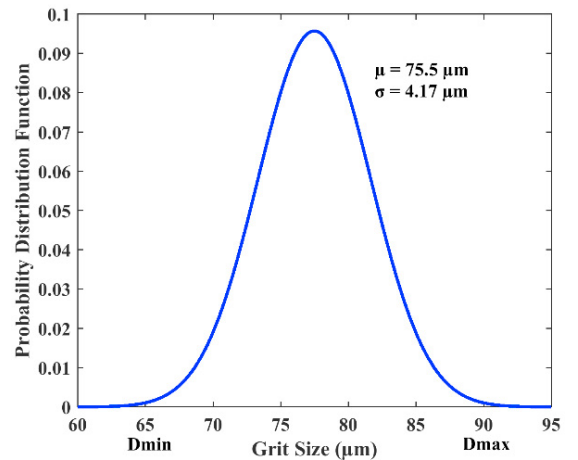
In the heat transfer module, the initial and boundary conditions are fixed. Heat transfer by conduction, convection and radiation are considered based on the equations (1), (2) and (3). User defined meshing of the geometric elements are chosen and free tetrahedral mesh shape is used. The minimum element size is optimized in order to avoid any error in meshing.

#### 4. Modeling and simulation of single-pulse laser ablation of grinding wheels

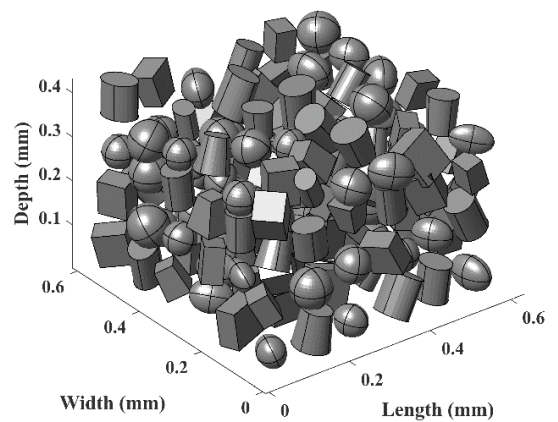
For the modeling work, resin bonded CBN and diamond wheels are chosen based on [5]. The specification of the wheels are CBNII180B100 and RVD180B100. The concentration of superabrasive in the grinding wheel is 100. This represents the volume fraction ( $V_g$ ) of CBN abrasive of 0.24 and diamond

abrasive of 0.25 in the respective grinding wheels [31]. Since the amount of porosity is negligible in resin bonded grinding wheels, the corresponding volume fractions of resin bond ( $V_b$ ) in the respective grinding wheels become 0.76 and 0.75 respectively. For the chosen grinding wheels, the maximum ( $D_{max}$ ) grit size and minimum ( $D_{min}$ ) grit size are given as 90  $\mu\text{m}$  and 65  $\mu\text{m}$  respectively. The average grit size ( $D_g$ ) is calculated as  $(D_{max} + D_{min})/2$ , which comes out to be about 77.5  $\mu\text{m}$ .

A six sigma normal distribution of grit sizes used to generate the resin bonded diamond grinding wheel structure for dimensions of 0.5 mm x 0.5 mm x 0.3 mm on MATLAB end based on the procedure discussed in the Section 3.1 is shown in Fig. 5.



(a)



(b)

Fig. 5. a) Normal distribution of grit size. b) Generation of grits



The model is then imported into the COMSOL end and the orientations of the grits are corrected to avoid any overlaps between grits. Then a few micron depth is sliced to represent trued wheel surface as shown in Fig.6(b).

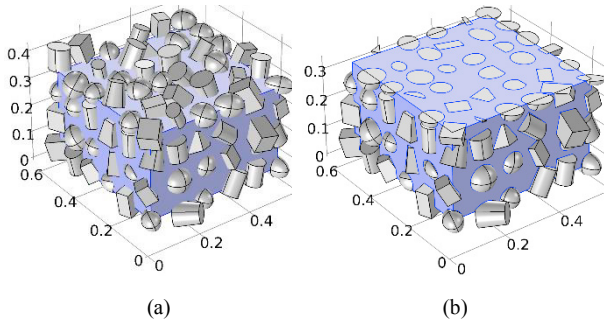


Fig. 6. a) Modeled wheel structure b) Trued wheel surface

In the heat transfer module, all the boundary conditions and initial condition were set. The initial temperature was kept at 293.15 K and boundary heat source was applied at the laser spot with Gaussian intensity distribution. The input parameters are given in Table 2. The material properties of the grits and bond domain elements were assigned based on the data from the literature as shown in Table 3. The temperature dependence of thermal conductivity and specific heat at constant pressure of both CBN and diamond as well as the density of phenolic resin is considered based on the literature [36, 39, 47, 45].

The meshing was kept at fine level and the minimum element size was kept as 10 nm. In the study node, the parametric study was performed with the intensity varying from  $10^{10}$  W/m<sup>2</sup> to  $1.2 \times 10^{11}$  W/m<sup>2</sup> with a step of  $10^{10}$  W/m<sup>2</sup>. The solver was run from the time range of 0 to  $1.2t_p$  with a step of  $0.02t_p$ . The results of the transient thermal model simulated for various intensity at the end of pulse duration for both resin bonded diamond and CBN wheels are obtained and the crater geometry are derived by removing the domain elements which had temperature higher than the vaporization temperatures of grit and bond in the respective domains. A slice is cut along a vertical plane passing through the center of laser spot to show the variation of crater geometry with intensity for single pulse laser irradiation for both wheels as shown in Fig. 7. The 3 D geometry of single-pulse laser ablated wheel surface at a laser intensity of  $1.2 \times 10^{11}$  W/m<sup>2</sup> is shown in Fig. 8. It can be seen that the crater depth is formed by the removal of bond without any damage to the grits.

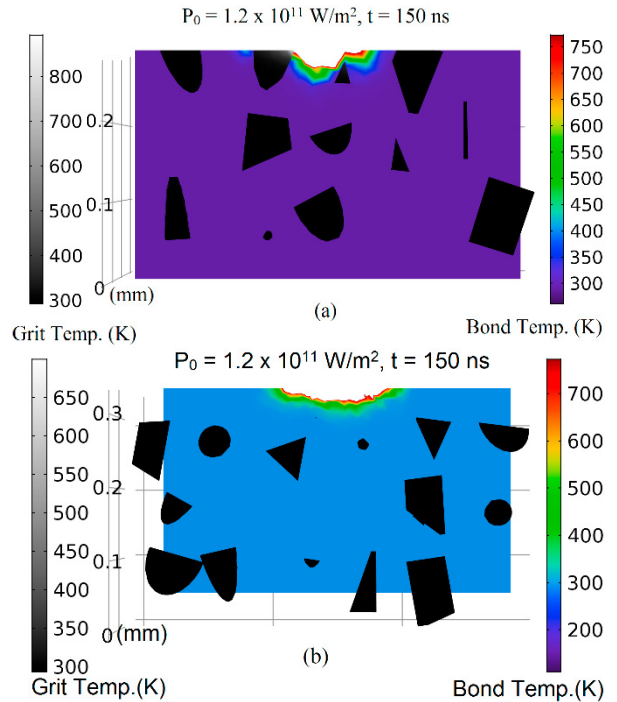


Fig. 7. 2 D Crater geometry formed due to single pulse laser ablation for intensity  $1.2 \times 10^{11}$  W/m<sup>2</sup> for a) Resin bonded CBN wheel b) Resin bonded diamond wheel

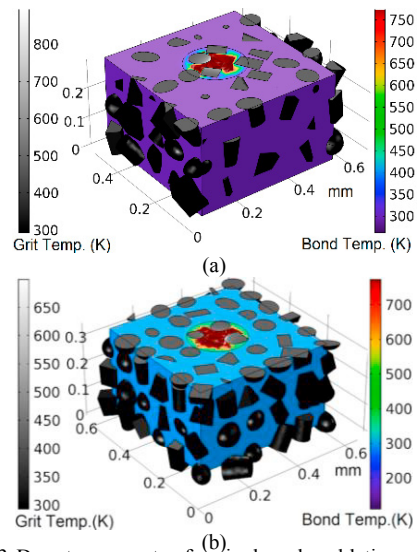


Fig. 8. 3 D crater geometry for single pulse ablation on a) Resin bonded CBN wheel b) Resin bonded diamond wheel at an intensity of  $1.2 \times 10^{11}$  W/m<sup>2</sup> at the end of one pulse width.

## 5. Results and discussion

The profile of crater formed due to vaporization of bond in a single pulse laser ablation along a vertical

plane passing through the center of laser spot for an intensity  $1.2 \times 10^{11} \text{ W/m}^2$  is shown in Fig. 7 for resin bonded CBN and diamond wheels. The geometry of crater formed depends on the average laser power and the focal offset. Besides this, the location of spot on the wheel surface influence the crater geometry. This is due to the random spatial distribution of grits in the volume of bond material. Modeling results are validated with the results published in the literature and post process analysis of the influence of laser dressing process parameters on the crater geometry is also discussed.

5.1. Validation of modeling results

A comparison of the modeled crater depth was made with the experimental results covered by Xie X Z et al 2004 [5]. Fig. 9 shows the maximum crater depth obtained by removing resin bond by vaporization. From Fig. 9, it can be noted that the maximum depth of crater matches with the experimental values at intensities upto  $4 \times 10^{10} \text{ W/m}^2$  and  $6 \times 10^{10} \text{ W/m}^2$  for CBN and diamond wheels respectively with errors of less than 25%, beyond which large deviations can be seen. Also it can be noted that the maximum crater

depth obtained due to bond removal by vaporization in single-pulse laser ablation is relatively more close to the experimental values at higher intensities for diamond wheel than that of CBN wheel. The observed deviations in the crater depth can be associated to the dynamics of molten phase during single-pulse laser ablation, which need to be addressed by future modeling efforts. Also the temperature dependence of the property of resin bond such as thermal conductivity and specific heat at constant pressure need to be considered. Besides this, the modeling needs to consider the plasma shielding effect as well as the cooling effect due to forced convection of co-axial gases used in laser ablation of grinding wheel.

5.2. Variation of material removal in a single pulsed laser ablation

The amount of material removed with time due to vaporization of bond is shown in Fig. 10(a). It can be observed that amount of material removed by vaporization during single pulse laser ablation for CBN wheel is relatively lower as compared to diamond wheel at certain initial time duration after which it grows more than that of diamond wheel.

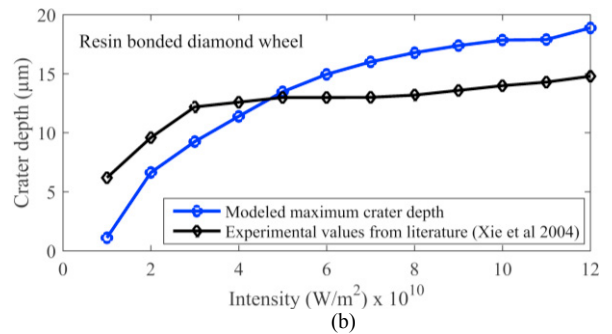
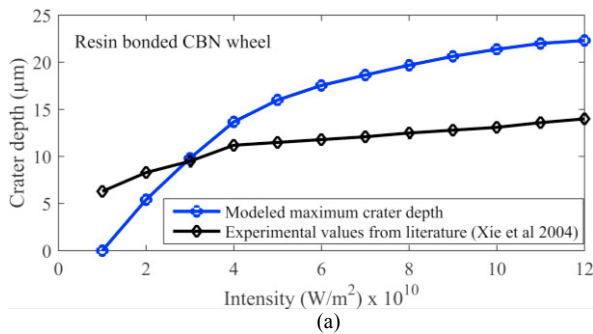


Fig. 9. Variation of maximum crater depth in single pulsed laser ablation with intensity ranging from  $10^{10} \text{ W/m}^2$  to  $1.2 \times 10^{11} \text{ W/m}^2$  for a) Resin bonded CBN wheel b) Resin bonded diamond wheel.

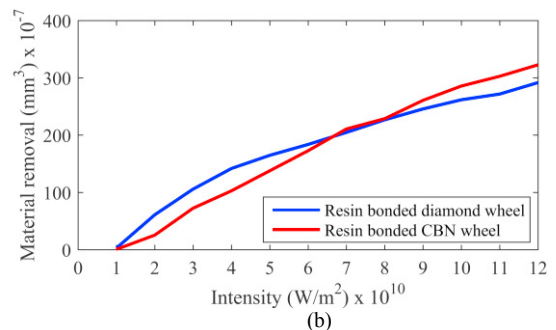
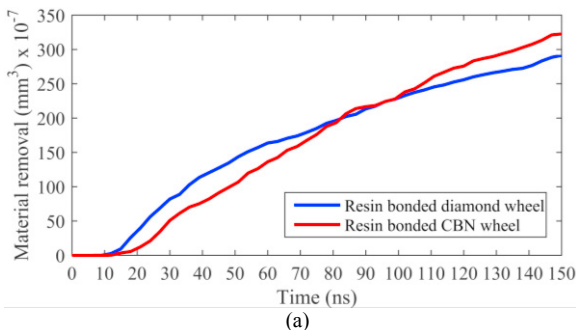


Fig. 10. a) Material removal with respect to time in single pulsed laser ablation for intensity of  $1.2 \times 10^{11} \text{ W/m}^2$ . b) Material removal with respect to intensity from  $10^{10} \text{ W/m}^2$  to  $1.2 \times 10^{11} \text{ W/m}^2$ .

This may be due to the increase of specific heat and decrease of thermal conductivity of diamond at higher temperature which decreases heat flux in the bond thereby reducing bond removal in diamond grinding wheel. Fig. 10(b) shows the variation of material removal with intensity at the end of one pulse. Here also the material removal in CBN wheel is lower than that of diamond at lower intensity and it shifts higher than diamond at certain higher intensity. This again may be due to the increase of specific heat capacity and decrease of thermal conductivity of diamond with the application of high intensities.

## 6. Conclusion

In this paper, a single-pulse laser ablation on resin bonded superabrasive grinding wheels was modeled by considering laser-wheel interaction over a period of one pulse width with varying levels of intensity. The variation of maximum crater depth with laser power density, varied from  $10^{10}$  W/m<sup>2</sup> to  $1.2 \times 10^{11}$  W/m<sup>2</sup>, was simulated for resin bonded CBN and diamond wheels using finite element based package COMSOL Multiphysics® 5.2. The predicted results are validated with the published results. It was noted that the predicted maximum depth of crater deviated from the experimental values at higher intensity range. The deviation in the modeling results is attributed to the dynamics of process during molten phase of resin bond especially at higher intensities, the effect of plasma shielding and the effect of cooling due to co-axial or inert gas used in laser ablation. The geometry of crater depends on the power density of laser and the thermo-physical and optical properties of grit and bond. Intensities higher than threshold intensity of bond and lower than the grit can effectively remove bond material. When the pulse intensity is sufficiently higher, it can damage both grit as well as bond. In this work, intensities lower than threshold intensity of grit were considered to cause bond removal in a single-pulse ablation. By using optimum set of the parameters, the desired crater geometry can be obtained. In laser dressing of grinding wheels, laser power density and feed rate influences the topography generated on wheel by laser irradiation. This model is an attempt to study the laser-wheel interaction during

laser dressing process for one pulse duration. Future attempts will be made to extend this model to predict the topography of laser dressed wheels.

## References

- [1] Fletcher NP, Maden H. The influence of diamond geometry on the stability of the grinding wheel dressing process. In Proceedings of the Nineteenth International Machine Tool Design and Research Conference 1979 (pp. 607-614). Macmillan Education UK.
- [2] Buttery TC, Statham A, Percival JB, Hamed MS. Some effects of dressing on grinding performance. *Wear*. 1979 Aug 1;55(2):195-219.
- [3] Babu NR, Radhakrishnan V, Murti YV. Investigations on laser dressing of grinding wheels—part I: preliminary study. *Journal of Engineering for Industry*. 1989 Aug 1;111(3):244-52.
- [4] Babu NR, Radhakrishnan V. Investigations on laser dressing of grinding wheels—part II: grinding performance of a laser dressed aluminum oxide wheel. *ASME J. Eng. Ind.* 1989 Aug 1;111:253-61.
- [5] Xie XZ, Chen GY, Li LJ. Dressing of resin-bonded superabrasive grinding wheels by means of acousto-optic Q-switched pulsed Nd: YAG laser. *Optics & Laser Technology*. 2004 Jul 31;36(5):409-19.
- [6] Yung KC, Chen GY, Li LJ. The laser dressing of resin-bonded CBN wheels by a Q-switched Nd: YAG laser. *The International Journal of Advanced Manufacturing Technology*. 2003 Nov 1;22(7-8):541-6.
- [7] Jackson MJ, Robinson GM. Development of morphology in laser dressed grinding wheels. *Journal of Achievements in Materials and Manufacturing Engineering*. 2007 May;22(1):81-4.
- [8] Harimkar SP, Dahotre NB. Evolution of Surface Morphology in Laser-Dressed Alumina Grinding Wheel Material. *International journal of applied ceramic technology*. 2006 Oct 1;3(5):375-81.
- [9] Jackson MJ, Robinson GM, Dahotre NB, Khangar A, Moss R. Laser dressing of vitrified aluminium oxide grinding wheels. *British Ceramic Transactions*. 2003 Dec 1;102(6):237-45.
- [10] Khangar A, Dahotre NB. Morphological modification in laser-dressed alumina grinding wheel material for microscale grinding. *Journal of materials processing technology*. 2005 Dec 14;170(1):1-0.
- [11] Chen M, Sun FH, Liu GL, Jian XG, Li XT. Theoretical and experimental research on generation mechanism of grinding wheel topography by laser dressing and 3D laser scanning. *InKey Engineering Materials 2003* (Vol. 233, pp. 497-502). Trans Tech Publications.
- [12] Chen M, Ma YP, Liu G, Xiang DH, Sun FH. Resin Bonded CBN Grinding Wheel Dressing by Laser—Simulation and Experiment. *InKey Engineering Materials 2006* (Vol. 304, pp. 38-42). Trans Tech Publications.
- [13] Hosokawa A, Ueda T, Yunoki T. Laser dressing of metal bonded diamond wheel. *CIRP Annals-Manufacturing Technology*. 2006 Jan 1;55(1):329-32.
- [14] Kunieda Y, Matsuura H, Kodama S, Yoshihara N, Yan JW, Kuriyagawa T. Development of a new laser conditioning method for ultra-fine grit diamond wheels. *InKey Engineering*

- Materials 2007 (Vol. 329, pp. 175-180). Trans Tech Publications.
- [15] Matsuura H, Hane K, Kunieda Y, Yoshihara N, Yan JW, Kuriyagawa T. Development of laser dresser for resin bonded diamond wheel. InKey Engineering Materials 2007 (Vol. 329, pp. 169-174). Trans Tech Publications.
- [16] Bathe R, Singh AK, Padmanabham G. Effect of pulsed laser dressing of metal-bonded diamond wheels on cutting performance. Materials and Manufacturing Processes. 2014 Mar 4;29(3):386-9.
- [17] Rabiey, M., Walter, C., Kuster, F., Stirnimann, J., Pude, F., & Wegener, K. Dressing of hybrid bond CBN wheels using short-pulse fiber laser. *Strojniški vestnik-Journal of Mechanical Engineering*, 2012, 58(7-8), 462-469.
- [18] Walter C, Rabiey M, Warhanek M, Jochum N, Wegener K. Dressing and truing of hybrid bonded CBN grinding tools using a short-pulsed fibre laser. *CIRP Annals-Manufacturing Technology*. 2012 Dec 31;61(1):279-82.
- [19] Deng H, Chen GY, Zhou C, Li SC, Zhang MJ. Processing parameter optimization for the laser dressing of bronze-bonded diamond wheels. *Applied Surface Science*. 2014 Jan 30;290:475-81.
- [20] Chen G, Cai S, Zhou C. On the laser-driven integrated dressing and truing of bronze-bonded grinding wheels. *Diamond and Related Materials*. 2015 Nov 30;60:99-110.
- [21] Cai S, Chen G, Zhou C. Research and application of surface heat treatment for multipulse laser ablation of materials. *Applied Surface Science*. 2015 Nov 15;355:461-72.
- [22] Song C, Genyu C, Cong Z, Hui D. The mechanism and application of bronze-bond diamond grinding wheel pulsed laser dressing based on phase explosion. *International Journal of Advanced Manufacturing Technology*. 2015 Oct 1;81.
- [23] Wang XY, Wu YB, Wang J, Xu WJ, Kato M. Absorbed energy in laser truing of a small vitrified CBN grinding wheel. *Journal of materials processing technology*. 2005 May 15;164:1128-33.
- [24] Wang XY, Wu YB, Kang RK, Guo DM, Xu WJ, Kato M. Energy Model in Laser Processing of a Cylindrical Grinding Wheel. InKey Engineering Materials 2006 (Vol. 304, pp. 33-37). Trans Tech Publications.
- [25] Wang XY, Kang RK, Xu WJ, Wang LJ, Guo DM. Modeling of Laser Dressing for Metal-bond Diamond Grinding Wheel. InKey Engineering Materials 2007 (Vol. 329, pp. 145-150). Trans Tech Publications.
- [26] Vora HD, Dahotre NB. Surface topography in three-dimensional laser machining of structural alumina. *Journal of Manufacturing Processes*. 2015 Aug 31;19:49-58.
- [27] Phanindranath V, Babu NR. A theoretical model for prediction of groove geometry on laser dressed grinding wheel surface. *International Journal of Machine Tools and Manufacture*. 1996 Jan 1;36(1):1-6.
- [28] Chen GY, Mei LF, Zhang B, Zhu DJ, Chen GG. Numerical simulation study on truing and dressing of bronze-bonded diamond wheel with pulsed laser. InKey Engineering Materials 2008 (Vol. 359, pp. 166-170). Trans Tech Publications.
- [29] Zahedi A, Tawakoli T, Azarhoushang B, Akbari J. Picosecond laser treatment of metal-bonded CBN and diamond superabrasive surfaces. *The International Journal of Advanced Manufacturing Technology*. 2015 Feb 1;76(5-8):1479-91.
- [30] Zhou C, Deng H, Chen G, Zhang Y, Wang D, Zhou X. Numerical simulation of single-pulse laser ablation for dressing a bronze-bond diamond grinding wheel. *Precision Engineering*. 2016 Jan 31;43:78-85.
- [31] Malkin, Stephen. *Grinding Technology*, Industrial Press, pg no. 14, 16 and 34, 2008.
- [32] Z.B. Hou, R. Komanduri, On the mechanics of the grinding process— Part I. Stochastic nature of the grinding process, *International Journal of Machine Tools and Manufacture*, 43 (15) (2003) 1579–1593.
- [33] Uma Shankar and N. Ramesh Babu, Digital Modeling of Grinding Wheel Structure, 10<sup>th</sup> International Conference Precision, Meso, and Nano Engineering, 07 – 09 Dec, 2017, Indian Institute of Technology Madras.
- [34] Lutey AH, Fortunato A, Zanini F, Carmignato S. Pulsed Laser Profiling of Grinding Wheels at Normal and Quasi-Tangential Incidence. *Lasers in Manufacturing and Materials Processing*. 2016 Sep 1;3(3):158-73.
- [35] <http://www.hppolymer.com/p84-binding-resin.php>.
- [36] Beiss, P., Ruthardt, R., & Warlimont, H. (2002). *Powder metallurgy data. refractory, hard and intermetallic materials*.
- [37] "Phenol Formaldehyde (PF, Phenolic)", [www.makeitfrom.com/material-properties/Phenol-Formaldehyde-PF-Phenolic](http://www.makeitfrom.com/material-properties/Phenol-Formaldehyde-PF-Phenolic), retrieved 2018-02-10.
- [38] Marinescu, I. D., Hitchiner, M. P., Uhlmann, E., Rowe, W. B., & Inasaki, I. (2006). *Handbook of machining with grinding wheels*. CRC Press.
- [39] Prelas, M. A., Popovici, G., & Bigelow, L. K. (Eds.). (1997). *Handbook of industrial diamonds and diamond films*. CRC Press.
- [40] Mei, L., Chen, G., Zhang, B., Chen, G., & Huang, K. (2009). Measurement of YAG laser absorptance by artificial diamond and cubic boron nitride. *Optics & Laser Technology*, 41(6), 770-777.
- [41] Slobodkin, L. S., & Flyaks, M. Y. (1987). Radiative properties of thermally protective materials based on phenolic asbestos-plastics. *Journal of Engineering Physics and Thermophysics*, 53(1), 791-795.
- [42] Neuberger, M. (2013). *III–V semiconducting compounds*. Springer Science & Business Media.
- [43] Zaitsev, A. M. (2013). *Optical properties of diamond: a data handbook*. Springer Science & Business Media.
- [44] Poerschke, R., & Madelung, O. (1991). *Data in Science and Technology, Semiconductors, Group IV Elements and III-V Compounds*. Berlin/Marburg: Springer-Verlag.
- [45] Ko, T. H., Kuo, W. S., & Chang, Y. H. (2001). Microstructural changes of phenolic resin during pyrolysis. *Journal of applied polymer science*, 81(5), 1084-1089.
- [46] [https://www.engineersedge.com/heat\\_transfer/convective\\_heat\\_transfer\\_coefficients\\_13378.htm](https://www.engineersedge.com/heat_transfer/convective_heat_transfer_coefficients_13378.htm)
- [47] Victor, A. C. (1962). Heat capacity of diamond at high temperatures. *The Journal of Chemical Physics*, 36(7), 1903-1911.